Inversion asymmetry, hole mixing, and enhanced Pockels effect in quantum wells and superlattices

Bang-fen Zhu* and Yia-Chung Chang
Department of Physics, University of Illinois at Urbana-Champaign, 1110 West Green Street, Urbana, Illinois 61801
(Received 27 May 1994)

The effects of inversion asymmetry on the anisotropic optical transition in the presence of electric field (Pockels effect) in GaAs/$Ga_{1-x}Al_xAs$ quantum wells and superlattices are investigated theoretically. Within an 8×8 $\mathbf{k} \cdot \mathbf{p}$ effective mass Hamiltonian formalism, in which the linear k, k^3, ϵ (strain due to the piezoelectric effect), ϵk, and Rashba terms are taken into account, we have derived the renormalized effective Hamiltonian for the electron and hole, respectively. The effects of the inversion asymmetry and the hole mixing on the spin-split subband structures and the dependence of optical transition matrix elements on the polarization of incident light are fully presented. The microscopic model clearly shows that the inversion asymmetry is responsible for the Pockels effect. The roles played by the hole mixing in the enhanced quantum well Pockels effect mediated by the electron-hole pairs are shown by our calculations. Thus we develop a theory with exciton states with eight spin components (due to the broken twofold degeneracy of the electrons) in the quantum well and calculate the excitonic spectra. The symmetry analysis and numerical results indicate that the excitonic anisotropic behavior results from the interference between different spin components of holes, which, owing to the heavy- and light-hole mixing, is enhanced significantly compared with the bulk material, especially for those exciton states whose dominant component does not coincide with its optically active component. Comparison between theory and experiment is discussed.

I. INTRODUCTION

Since the mid 1980s there has been extensive interest in the effects of an applied electric field normal to the layers on the optical properties of semiconductor multiple quantum wells (MQW's) and superlattices (SL's), which manifests itself mostly in two aspects. On the one hand, the quantum confinement due to the potential barrier prevents the exciton from electric-field-induced dissociation, leading to the quantum-confined Stark effect in MQW's; on the other hand, owing to the larger superperiod and the smaller mini-Brillouin zone, a moderate field intensity is enough to produce Wannier-Stark ladders and Bloch oscillations in superlattices, and thereby the corresponding optical spectra.

Recently, Kwok *et al.* measured the biaxial response of photoluminescence (PL) to electric fields in a GaAs/$Ga_{1-x}Al_xAs$ quantum well structure.[1] They found that (1) for fields along [001], emission due to some nominally forbidden excitons exhibits substantial differences between $[1\bar{1}0]$ and [110] polarizations, but not between [100] and [010] polarizations, and no noticeable anisotropy is observed for the "allowed transitions;" (2) the field dependence of the anisotropy is antisymmetric and its magnitude decreases with increasing field. They ascribe their observation to the Pockels linear electrorefraction effect in quantum wells.

It is well known that the indicatrix (an ellipsoid describing the dielectric constant tensor) for a cubic crystal is normally a sphere and, since all central sections are circles, there is no natural double refraction. If an external electric field is applied to this system, in general, the indicatrix will be perturbed to some extent, which is known as the electro-optic effect. Such a change can generally be expanded in terms of the applied field. Suppose that the cubic crystal has a center of inversion. If the field is reversed in direction, the physical situation is essentially unaltered so that no linear perturbation in the refractive index due to the field exists. However, in zinc-blende semiconductors, unlike a centrosymmetrical crystal, there is no reason why reversing the field should not change the refractive index, and so the linear change of the refractive index with respect to the field would remain. The electric-field-induced biaxial birefringence within the plane perpendicular to the field is known as the Pockels effect.[2] Suppose an electric field is applied along the z direction, in the x-y plane the refraction index can be altered by an amount up to δn, proportional to the field F. If we select two mutually perpendicular directions x' and y' (e.g., $[1\bar{1}0]$ and [110] for GaAs), such that $n_{x'} = n + \delta n$ and $n_{y'} = n - \delta n$, the Pockels coefficient r_{41} is defined by $2\delta n = r_{41} n^3 F$. For a stress-free sample, the observed electro-optic effect is the sum of the primary effect (i.e., the electro-optic effect for a strain-free sample) and secondary effect (i.e., the photoelastic effect caused by the field-induced strain via the converse piezoelectric effect). According to an estimation for bulk material, the secondary effect is comparable in magnitude to the primary effect.[2]

This electro-optic (Pockels) effect is usually very small

up to the breakdown field (10^6 V cm^{-1}) for most III-V group compound semiconductors. For example, below the energy gap, the experimental Pockels coefficient r_{41} on bulk GaAs is about 1.5×10^{-10} cm/V, i.e., $(\partial n/\partial F)_{F=0} = 10^{-8}$ cm/V. The most interesting point in Kwok *et al.*'s paper is that the observed polarization ratio (the difference between the PL intensities along the $[1\bar{1}0]$ and $[110]$ directions over the summation) is as large as 20 – 30%, several orders of magnitude larger than the corresponding bulk values. Besides, this giant Pockels effect unusually *decreases* in anisotropy with increasing field. Clearly, as believed by these authors, it can only be accounted for by the quantum well effects.

By macroscopic symmetry analysis, the bulk Pockels effect has been considered to be a consequence of the inversion asymmetry. However, there seems to be little theoretical effort toward the understanding of the microscopic details of this effect even for bulk materials, though there is some suggestion that the Pockels effect is related to the higher order $\mathbf{k} \cdot \mathbf{p}$ terms.[3] As for MQW's or SL's, to our knowledge, no theory has been reported on the anisotropic electro-optic effects. In this paper we intend to present a theoretical formulation for the quantum well Pockels effect, and, in particular, to show how the quantum well effect enhances the in-plane optical anisotropy by microscopic calculations.

The article is organized as follows. In Sec. II, a multiband electron and hole Hamiltonian suitable to describe the superlattice Pockels effect is presented. Although many sophisticated techniques are powerful for band structure calculation of bulk materials in which the full effects due to the inversion asymmetry are included,[4] to deal with the present issue, namely, a long-period superlattice in the presence of an external electric field as well as its associated converse piezoelectric effect, we prefer starting from a semiempirical $\mathbf{k} \cdot \mathbf{p}$ multiband Hamiltonian.[5,6] It is not only more transparent and easy to interpret, but also proves effective and feasible for quantum well and superlattice problems.[7–10] In addition to the usual quadratic (k^2) terms and the superlattice potential, this Hamiltonian also contains various inversion-asymmetry-related terms, such as the linear k term, cubic k^3 term, linear ϵ term (the strain caused by the converse piezoelectric effect for free samples), ϵk term, and the Rashba term which allows for the electric-field-induced coupling between band states. Numerical results for spin splitting of the superlattice conduction and valence subbands in the presence of an external electric field are given in Sec. III, in which the contribution from each inversion-asymmetry-related term is illustrated. Although the in-plane fourfold symmetry of the subband structure is broken by the inversion asymmetry, some symmetry properties are preserved. The relation of these remaining symmetry properties to the polarization dependence of the optical spectra is discussed. The anisotropic optical spectra due to hole-electron subband transition are shown in Sec. IV. The hole mixing effects on the anisotropic interband transitions are conclusively shown. Since the excitons play an important role in quantum well and superlattice optical processes, a special emphasis is placed on the effects of inversion asymmetry on the exciton structure and the excitonic optical transitions in Sec. V. The field dependence of the polarization ratio, the binding energies, and the oscillator strengths for several allowed and forbidden exciton states is presented. Finally, a comparison between experiment and theory is discussed and conclusions are drawn.

II. HAMILTONIAN

A. Bulk effective Hamiltonian

The $\mathbf{k} \cdot \mathbf{p}$ method is commonly used to obtain the perturbation expansion, quadratic in k, of bands around high-symmetry points.[5,6] In order to obtain the $\mathbf{k} \cdot \mathbf{p}$ Hamiltonian, one common practice is to separate the states concerned in the perturbation calculation into two sets, one of which involves several quasidegenerate states whose interaction is treated exactly, and the other contains those which are well removed in energy from the first set, and interact with it weakly.[11] In the present instance, since we are most interested in the optical processes near the fundamental gap, the eightfold subspace of Γ_6^c, Γ_8^v, and Γ_7^v is suitable in the first category, while other bands, such as Γ_8^c, Γ_7^c, and some more remote bands, belong to the second set. Generally speaking, the 8×8 $\mathbf{k} \cdot \mathbf{p}$ solution is accurate for the near-fundamental-gap states with wave number less than $0.03\frac{2\pi}{a_0}$,[12] which are sufficient to describe the wave functions of the low-lying electron and hole subbands for a typical MQW with well width around 100 Å. Although the accuracy region provided by the 8×8 Hamiltonian is a little smaller than the region we are interested in, yet it is more feasible and we believe it will not lead to any qualitative error. There have been several extensive theoretical studies on the $\mathbf{k} \cdot \mathbf{p}$ Hamiltonian in bulk zinc-blende materials in which the inversion asymmetry effects are taken into account.[4,5,12–14] There are also several papers devoted to the effects of the inversion asymmetry in SL's or MQW's based on the multiband effective Hamiltonian. Most of them focused on the electrons, such as the electron cyclotron resonance in a magnetic field,[15] the nonparabolicity and the g factors of the electrons,[16] the electron spin splitting,[16–18] and the spin-flip scattering.[19] Since we shall concentrate on the interband optical transition in superlattices subject to an applied electric field and it seems to us that no single Hamiltonian meets all the requirements of the present issue adequately and consistently, we will first briefly introduce our multiband Hamiltonian for bulk materials, and then present the appropriate Hamiltonian for superlattice electrons and holes.

The basis functions used are denoted by $|\Gamma_6^c, \uparrow\rangle$, $|\Gamma_6^c, \downarrow\rangle$, $|\Gamma_8^v, \frac{3}{2}\rangle$, $|\Gamma_8^v, \frac{1}{2}\rangle$, $|\Gamma_8^v, -\frac{1}{2}\rangle$, $|\Gamma_8^v, -\frac{3}{2}\rangle$, $|\Gamma_7^v, \frac{1}{2}\rangle$, and $|\Gamma_7^v, -\frac{1}{2}\rangle$, which are related to the zone-center Bloch states $|S\rangle, |X\rangle, |Y\rangle, |Z\rangle$ and the electron spinors as given in Ref. 5. Our 8×8 matrix Hamiltonian, whose rows and columns are ordered as specified above, is expressed as

$$\begin{pmatrix} E_g + A' & 0 & \sqrt{3}K_+ & -\sqrt{2}K_z & -K_- & 0 & K_z & \sqrt{2}K_- \\ & E_g + A' & 0 & K_+ & -\sqrt{2}K_z & -\sqrt{3}K_- & \sqrt{2}K_+ & -K_z \\ & & F' & H' + J' & I' + Ck_z & -\frac{\sqrt{3}}{2}Ck_- & -\frac{H'+J'}{\sqrt{2}} & -\sqrt{2}I' + \frac{C}{\sqrt{2}}k_z \\ & & & G' & \frac{\sqrt{3}}{2}Ck_+ + iD'k_- & I' - Ck_z & \frac{F'-G'}{\sqrt{2}} & \sqrt{\frac{3}{2}}H' - L' \\ & & & & G' & -H' + J' & \sqrt{\frac{3}{2}}H'^* + L'^* & -\frac{F'-G'}{\sqrt{2}} \\ & & \text{c.c.} & & & F' & \sqrt{2}I'^* + \frac{C}{\sqrt{2}}k_z & \frac{J'^*-H'^*}{\sqrt{2}} \\ & & & & & & \frac{F'+G'}{2} - \Delta & 0 \\ & & & & & & & \frac{F'+G'}{2} - \Delta \end{pmatrix}, \tag{1}$$

where c.c. denotes the complex conjugate of the corresponding matrix element, the energy of Γ_8^v is taken to be zero, and E_g and Δ are the energies of the fundamental gap and the zone-center spin-orbit splitting of the Γ_{15}^v valence band, respectively. Let $k_\pm = k_x \pm ik_y$, and $k^2 = k_x^2 + k_y^2 + k_z^2 = k_\parallel^2 + k_z^2$. The parameters A', F', G', H', and I' in the above expression are identical to the usual multiband Hamiltonian without the inversion asymmetry, which mainly originates from the second-order process perturbed by the $\mathbf{k}\cdot\mathbf{p}$ term except for I' which also contains the first-order intraband perturbation by the strain Hamiltonian. We have

$$A' = \left(\frac{\hbar}{m_0}\right)^2 \left\{ \sum_j{}' \frac{|\langle S|\mathbf{k}\cdot\mathbf{p}|U_j\rangle|^2}{E_g - E_j} + \frac{m_0 k^2}{2} \right\}, \tag{2}$$

$$F' = -\frac{\hbar^2}{2m_0}\{(\gamma_1' + \gamma_2')k_\parallel^2 + (\gamma_1' - 2\gamma_2')k_z^2\}, \tag{3}$$

$$G' = -\frac{\hbar^2}{2m_0}\{(\gamma_1' - \gamma_2')k_\parallel^2 + (\gamma_1' + 2\gamma_2')k_z^2\}, \tag{4}$$

$$H' = \frac{\sqrt{3}\hbar^2}{m_0}\gamma_3' k_z k_-, \tag{5}$$

$$I' = \frac{\sqrt{3}\hbar^2}{2m_0}\{\gamma_2'(k_x^2 - k_y^2) - i2\gamma_3' k_x k_y\} + id\epsilon, \tag{6}$$

where γ_1', γ_2', and γ_3' are obtained from the corresponding Luttinger band parameters[6] γ_1, γ_2, and γ_3 minus the contribution from the Γ_1^c band. ϵ is the shear strain in the x-y plane caused by an external electric field F along the z direction, which will be the only type of strain discussed in our paper, and $\epsilon = d_{14}F$, where d_{14} is the piezoelectric constant for the material studied. d is the valence band deformation potential constant defined by

$$d\epsilon = \langle X|\delta H_{\text{strain}}|Y\rangle/\sqrt{3}, \tag{7}$$

where δH_{strain} is the strain Hamiltonian.[3]

In the Hamiltonian above, $K_\pm$ and K_z, as composite terms, are defined by

$$K_\pm = \frac{1}{\sqrt{6}}\{i\overline{P}k_\pm \pm iBk_z k_\mp \mp eFB'k_\pm\}, \tag{8}$$

and

$$K_z = \frac{1}{\sqrt{3}}\{i\overline{P}k_z + Bk_x k_y + C_2\epsilon + eFR\}. \tag{9}$$

In addition to the matrix element of momentum operator $\mathbf{p}$ between the Γ_{15}^v and Γ_1^c bands, namely,

$$\overline{P} = -i\frac{\hbar}{m_0}\langle S|p_x|X\rangle, \tag{10}$$

and the interband deformation potential

$$C_2\epsilon = \langle Z|\delta H_{\text{strain}}|S\rangle = 2\sqrt{3}d^{v,cs}\epsilon, \tag{11}$$

there are two inversion-asymmetry-related terms.

(1) The interaction parameter B represents the indirect coupling between the valence and conduction band at the fundamental gap mediated by the remote band states, especially the Γ_{15}^c states, which would be forbidden if the inversion symmetry were retained. B reads

$$B = 2\left(\frac{\hbar}{m_0}\right)^2 \sum_j{}' \frac{\langle S|p_x|U_j\rangle\langle U_j|p_y|Z\rangle}{E_g/2 - E_j}. \tag{12}$$

(2) Both the parameters R and B' result from the matrix elements by the electric field, which was originally considered to be responsible for the spin splitting in the subbands. These so-called Rashba terms are proportional to $(\mathbf{k}\times\mathbf{F})\cdot\sigma$ (spin matrix),[15–17] and describe the field-induced direct coupling between the Γ_1^c and Γ_{15}^v states. We have

$$eFR = \langle S|eFz|Z\rangle = eF\overline{P}/E_g. \tag{13}$$

The field-induced coupling between the Γ_1^c and remote states, say the Γ_{15}^c, combined with the $\mathbf{k}\cdot\mathbf{p}$ interaction, is expressed as

$$eFB' = -i\frac{\hbar}{m_0}\sum_j{}' \frac{\langle S|eFz|Z_j'\rangle\langle Z_j'|p_x|Y\rangle}{E_g/2 - E_j}. \tag{14}$$

In the effective Hamiltonian above we allow for the inversion-asymmetry-related linear k terms, which appear as the terms containing parameter C in the Hamiltonian as well as in the following expressions:

$$J' = -\frac{C}{2}k_+ + i\frac{\sqrt{3}}{2}D'k_-, \tag{15}$$

$$L' = \sqrt{\frac{3}{8}}Ck_+ + i\frac{D'}{\sqrt{8}}k_-. \tag{16}$$

Kane listed three possible types of C: C^a, C^b, and C^c,[5] in which the first one arises from the first-order perturbation by the spin-orbit interaction Hamiltonian, H_{SO}, and

the other two result from the combined action of $\mathbf{k}\cdot\mathbf{p}$ and H_{SO}. As pointed out by Rossler,[12] C^a could not be finite because

$$\langle X|\frac{\partial V}{\partial y}|Z\rangle = i\langle X|[p_y, H]|Z\rangle = 0,$$

in which $\partial V/\partial y$ is proportional to the spin-orbit interaction Hamiltonian. Cardona conjectured that for most III-V semiconductors, contribution from C^c is negligible because the intermediate states required in this second-order perturbation process should be Γ_{25}-like and not available.[4] Thus, we have the same parameter C in both the diagonal submatrix of the Γ_8^v states and the nondiagonal block between Γ_8^v and Γ_7^v, otherwise these two parameters would differ by $1.5C^c$. So

$$C \propto \sum_j^{\Gamma_{12}} \frac{\langle X|p_x|U_j\rangle\langle U_j|[\nabla V \times p]_y|Y\rangle}{E_{\Gamma_{15}^v} - E_j}. \tag{17}$$

According to Ref. 4, C^b is produced by the second-order process in which the intermediate states are mainly the outmost core d levels.

Besides, in semiconductors with inversion asymmetry, a simultaneous interaction between the Γ_1^c and Γ_{15}^v states by the $\mathbf{k}\cdot\mathbf{p}$ and the strain Hamiltonian is possible. The latter is characterized by the parameter

$$iD' = iC_5'\epsilon = -\frac{4\hbar}{3m_0}\sum_j{}' \frac{\langle X|p_x|U_j\rangle\langle U_j|\delta H_{\text{strain}}|Y\rangle}{E_{\Gamma_{15}^v} - E_j}. \tag{18}$$

In deriving the above effective Hamiltonian and the associated parameters, as emphasized by Cardona,[4] great attention must be paid to a consistent definition of all these matrix elements. Following Ref. 4, we use a convention that the anion is chosen at the origin while the cation is at $(a_0/4)(1,1,1)$; then, with the phases of all the orbital wave functions chosen as real numbers, $\overline{P}$ as defined in Eq. (13) and Q and P' as defined below are positive numbers. Here

$$P' = -i\frac{\hbar}{m_0}\langle S|p_x|\Gamma_{15,X}^c\rangle, \tag{19}$$

$$Q = i\frac{\hbar}{m_0}\langle X|p_y|\Gamma_{15,Z}^c\rangle. \tag{20}$$

This convention is opposite to that implied by the measured polarization ratio in the experiment.[1]

B. Conduction electron Hamiltonian

Both the conduction and valence electron Hamiltonians are obtained from the 8×8 Hamiltonian by second-order perturbation theory via the nondiagonal submatrix blocks. In other words, we use the block between Γ_6^c and Γ_8^v (or Γ_7^v) as the perturbation operator to obtain the conduction band Hamiltonian and the block between Γ_8^v and Γ_6^c (or Γ_7^v) to obtain the valence band Hamiltonian. We consider the quantity k^n to be of the nth order and ϵ, eFR, eFB', and C to be of the second order. Thus, if only the quantities up to the third order are retained and higher order ones dropped, the renormalized 2×2 matrix for the conduction electron becomes

$$H_e^{(0)} = \begin{pmatrix} E_g + \frac{\hbar^2k^2}{2m^*} + T' & -U' \\ -U'^* & E_g + \frac{\hbar^2k^2}{2m^*} - T' \end{pmatrix}, \tag{21}$$

where

$$T' = \frac{2B\overline{P}}{3E_g}\frac{\Delta}{E_g+\Delta}k_z(k_x^2 - k_y^2), \tag{22}$$

$$U' = \frac{2B\overline{P}}{3E_g}\frac{\Delta}{E_g+\Delta}\left[k_z^2k_+ - ik_-\left(k_xk_y + \frac{C_2\epsilon + eFR}{B}\right)\right]. \tag{23}$$

It is easy to obtain the eigensolution to this 2×2 matrix. With the inversion asymmetry taken into account, the eigenvalue for the conduction electron associated with a given wave vector is

$$\begin{aligned} E_\pm &= E_g + \frac{\hbar^2k^2}{2m^*} \pm [|T'|^2 + |U'|^2]^{\frac{1}{2}} \\ &= E_g + \frac{\hbar^2k^2}{2m^*} \pm \frac{2B\overline{P}k_\parallel}{3E_g}\frac{\Delta}{E_g+\Delta}\left[k_z^2k^2 + k_\parallel^2(k_\parallel^2 - 8k_z^2)\frac{1-\cos 4\theta}{8} - k_z^2\sin 2\theta\frac{C_2\epsilon + eFR}{B} + \left(\frac{C_2\epsilon + eFR}{B}\right)^2\right]^{\frac{1}{2}}. \end{aligned} \tag{24}$$

We denote the angle between the two-dimensional (2D) wave vector of an electron and the x axis by θ and let $\mathbf{k}_\parallel = (k_\parallel, \theta)$. The corresponding eigenvectors now read

$$|\mathbf{k},1\rangle e^{\mathbf{k}\cdot\mathbf{r}} = \begin{pmatrix} [\frac{1+\chi(\mathbf{k})}{2}]^{\frac{1}{2}} \\ -\frac{U'^*}{|U'|}[\frac{1-\chi(\mathbf{k})}{2}]^{\frac{1}{2}} \end{pmatrix} e^{\mathbf{k}\cdot\mathbf{r}} \tag{25}$$

and

$$|\mathbf{k},2\rangle e^{\mathbf{k}\cdot\mathbf{r}} = \begin{pmatrix} -[\frac{1-\chi(\mathbf{k})}{2}]^{\frac{1}{2}} \\ -\frac{U'^*}{|U'|}[\frac{1+\chi(\mathbf{k})}{2}]^{\frac{1}{2}} \end{pmatrix} e^{\mathbf{k}\cdot\mathbf{r}}, \tag{26}$$

where $\chi(\mathbf{k}) = T'/U'$. Based on the 2×2 matrix H_e^0 it is straightforward to construct the superlattice electron Hamiltonian $\mathbf{H}_e$ just by adding the superlattice and the external electric potentials to the diagonal elements of the matrix, and replacing k_z with the operator $-i\partial/\partial z$.

We assume that (1) the band-edge functions of both $Ga_{1-x}Al_xAs$ and GaAs are identical, which is reasonable within the multiband envelope function formalism; (2) the barrier is so high and thick that it will bring in only a minor error by cutting the electric potential at the barrier center and repeating it periodically. Thus the

superlattice potential under the electric field has the form

$$V_e(z+nL) = V_e(z) = \begin{cases} eFz, & |z| \le \frac{W}{2}, \\ V_0^e + eFz, & \frac{W}{2} \le |z| \le \frac{L}{2}, \end{cases} \tag{27}$$

where L is the superlattice period, W is the well width, and V_0^e is the potential barrier height for electrons. The second assumption has been applied to calculate the subband structure in $Ga_{1-x}Al_xAs/GaAs$ multiple quantum wells in the presence of an electric field and the result was found to agree well with the results obtained by using the transfer matrix method.[20] The assumptions have also been used to study the excitonic optical transition in $GaAs/Ga_{1-x}Al_xAs$ multiple quantum wells as a function of the field strength and proved sound by comparison with experiment.[24]

Thus, since the potential $V_e(z)$ has the superlattice periodicity, only coupling between these bulk solutions whose k_z's differ by mK is possible, where m is an integer and K is the primitive superlattice reciprocal lattice vector along the z direction, i.e., $K = 2\pi/L$. Consequently, the envelope function of the μth conduction subband state associated with the superlattice wave vector $\mathbf{k}_e$ can be expanded in terms of the bulk solutions as

$$\phi_\mu(\mathbf{k}_e) = \exp[i\mathbf{k}_\parallel \cdot \rho_e + iqz_e] \times \sum_{m,i} a_{\mu,m,i} \exp(imKz)|\mathbf{k}_e, i\rangle, \tag{28}$$

where (ρ_e, z_e) is the coordinate of the electron and $\mathbf{k}_\parallel$ and q are the projections of the superlattice wave vector in the x-y plane and on the z axis, respectively. In this way, we avoided the difficulty of matching boundary conditions across the interfaces arising from the higher order differential operator of $-i\partial/\partial z$.[9]

The matrix element of the electron Hamiltonian $\mathbf{H}_e$ between two bulk solutions can be written as

$$\begin{aligned} &\langle \mathbf{k}_\parallel', q' + m'K, i'|\mathbf{H}_e|\mathbf{k}_\parallel, q + mK, i\rangle \\ &= \delta_{\mathbf{k}_\parallel,\mathbf{k}_\parallel'}\delta_{q,q'}\left(\left\{E_g + \frac{\hbar^2}{2m^*}[k_\parallel^2 + (mK+q)^2] \pm [|T'|^2 + |U'|^2]^{\frac{1}{2}} + V_0^e\frac{L-W}{L}\right\}\delta_{m,m'}\delta_{j,j'}\right. \\ &\left. + \langle \mathbf{k}_\parallel', q' + m'K, i'|\mathbf{k}_\parallel, q + mK, i\rangle \left\{-V_0^e\frac{\sin[(m-m')\pi W/L]}{(m-m')\pi} + ieFL\frac{(-1)^{m-m'}}{2(m-m')\pi}\right\}(1-\delta_{m,m'})\right). \end{aligned} \tag{29}$$

By solving the secular equation, we get the superlattice electron subband structure and the corresponding two-component wave function in an electric field, with the inversion-asymmetry effects included.

C. Hole Hamiltonian

Following a similar procedure as described in the last subsection, we construct a renormalized 4×4 valence electron Hamiltonian from the 8×8 matrix by keeping all quantities up to the third order. It is not easy to get the analytical eigensolutions to this renormalized 4×4 matrix, so we divide it into two parts: one is just the Kohn-Luttinger Hamiltonian denoted by $H_v^{(0)}$,[22] and the remainder is denoted by $H_v^{(1)}$.

$$\begin{aligned} \mathbf{H}_v &= \begin{pmatrix} F-T & H+\frac{\sqrt{3}}{2}U-\frac{C}{2}k_+ & I''+Ck_z & -\frac{\sqrt{3}}{2}Ck_- \\ & G-\frac{T}{3} & U+\frac{\sqrt{3}}{2}Ck_+ & I''-Ck_z \\ & & G+\frac{T}{3} & -H+\frac{\sqrt{3}}{2}U-\frac{C}{2}k_+ \\ & \text{c.c.} & & F+T \end{pmatrix} \\ &= \begin{pmatrix} F & H & I & 0 \\ & G & 0 & I \\ & & G & -H \\ & \text{c.c.} & & F \end{pmatrix} + \begin{pmatrix} -T & \frac{\sqrt{3}}{2}U-\frac{C}{2}k_+ & id\epsilon+Ck_z & -\frac{\sqrt{3}}{2}Ck_- \\ & -\frac{T}{3} & U+\frac{\sqrt{3}}{2}Ck_+ & id\epsilon-Ck_z \\ & & \frac{T}{3} & \frac{\sqrt{3}}{2}U-\frac{C}{2}k_+ \\ & \text{c.c.} & & T \end{pmatrix} \\ &\equiv \mathbf{H}_v^{(0)} + \mathbf{H}_v^{(1)}, \end{aligned} \tag{30}$$

where the terms F, G, H, and I'' have the identical expressions with the corresponding F', G', H', and I' as shown in Sec. II A, except that all the parameters of γ_1', γ_2', γ_3' in these expressions are replaced by the true Luttinger parameters γ_1, γ_2, γ_3. The term I in the expression of $\mathbf{H}_v^{(0)}$ is the same as I'' with $id\epsilon$ excluded. The terms U and T here are somewhat different from U' and T' of Sec. II A.

$$U = \frac{2B\overline{P}}{3E_g}\left[k_z^2k_+ - ik_-\left(k_xk_y + \frac{eFR}{B}\right)\right] + iC_5\epsilon k_-, \tag{31}$$

where

$$C_5 = C_5' - \frac{2C_2\overline{P}}{3E_g}; \tag{32}$$

$$T = \frac{2B\overline{P}}{3E_g} k_z(k_x^2 - k_y^2). \tag{33}$$

In a similar way, the superlattice hole Hamiltonian is derived by replacing all the k_z terms by $-i\partial/\partial z$ and adding the diagonal superlattice and electric potentials. For the sake of convenience, we reverse the sign of all the matrix elements. Expressing the superlattice potential for a hole under the electric field as

$$V_h(z+nL) = V_h(z) = \begin{cases} -eFz, & |z| \le \frac{W}{2}, \\ V_0^h - eFz, & \frac{W}{2} \le |z| \le \frac{L}{2}, \end{cases} \tag{34}$$

we have the superlattice hole Hamiltonian

$$\mathbf{H}_h \equiv \mathbf{H}_h^{(0)} + \mathbf{H}_h^{(1)} \equiv \{-\mathbf{H}_v^{(0)} + V_h\} - \mathbf{H}_v^{(1)}. \tag{35}$$

The electron and hole states are worked out in different ways: the basis functions for the former are bulk electron states with the inversion-asymmetry effects included; while for the latter we first solve the eigenequation of $H_h^{(0)}$,

$$\mathbf{H}_h^{(0)}\psi_\nu^{(0)}(\mathbf{k}_h) = E_\nu^{(0)}(\mathbf{k}_h)\psi_\nu^{(0)}(\mathbf{k}_h), \tag{36}$$

and then we include the effects of the inversion asymmetry. Let the hole wave function be expressed as

$$\psi_\nu(\mathbf{k}_h) = \sum_{\nu'} b_{\nu,\nu'}\psi_{\nu'}^{(0)}(\mathbf{k}_h). \tag{37}$$

The hole states are obtained by solving the following secular equation:

$$\det\left|(E_\nu^{(0)} - E)\delta_{\nu,\nu'} + \sum_{\nu'}\langle\psi_\nu^{(0)}|\mathbf{H}_h^{(1)}|\psi_{\nu'}^{(0)}\rangle\right| = 0. \tag{38}$$

It can be proved that a pair of nearly degenerate hole wave functions of $\mathbf{H}_h^{(0)}$ with wave vector $\mathbf{k}_h = (\mathbf{k}_\parallel, q)$ can be generally expressed in the Γ_8^v representation as

$$\psi_\nu^{(0)}(\mathbf{k}_h) = \begin{pmatrix} \alpha_\nu(\mathbf{k}_\parallel,q,z)\Delta_1 \\ \beta_\nu(\mathbf{k}_\parallel,q,z)\Delta_2 \\ i\beta_\nu(\mathbf{k}_\parallel,q,z)\Delta_3 \\ -i\alpha_\nu(\mathbf{k}_\parallel,q,z)\Delta_4 \end{pmatrix} \exp(i\mathbf{k}_h\cdot\mathbf{r}) \tag{39}$$

and

$$\psi_{\overline{\nu}}^{(0)}(\mathbf{k}_h) = \begin{pmatrix} \overline{\alpha}_\nu(\mathbf{k}_\parallel,q,z)\Delta_1 \\ -\overline{\beta}_\nu(\mathbf{k}_\parallel,q,z)\Delta_2 \\ i\overline{\beta}_\nu(\mathbf{k}_\parallel,q,z)\Delta_3 \\ i\overline{\alpha}_\nu(\mathbf{k}_\parallel,q,z)\Delta_4 \end{pmatrix} \exp(i\mathbf{k}_h\cdot\mathbf{r}). \tag{40}$$

Here Δ_j (j=1,4) are phase factors

$$\Delta_j = (e^{-i\theta}, 1, e^{-i\theta-i\eta}, e^{-i\eta}), \tag{41}$$

in which η is the phase angle of the complex function I in the zeroth-order Hamiltonian of the hole. To distinguish two near-degenerate states, we add a bar to one of the states which has the symmetry as shown in Eq. (40). Hereafter, if necessary, we may denote two near-degenerate hole states from the νth subband by indices ν and $\overline{\nu}$, respectively. All the spin-component functions of the hole, α, $\overline{\alpha}$, β, and $\overline{\beta}$ are expanded in terms of plane waves differing by a superlattice reciprocal wave vector. Inserting them into the Eqs. (37), (39), and (40), the zero-order hole wave functions (with the inversion asymmetry ignored) in the MQW in the presence of an electric field are obtained.

The wave function $\psi_\nu^{(0)}$ has the following in-plane symmetry

$$E_\nu^{(0)}(\theta) = E_\nu^{(0)}\left(\frac{\pi}{2} - \theta\right) = E_\nu^{(0)}(-\theta) = E_\nu^{(0)}\left(\frac{\pi}{2} + \theta\right), \tag{42}$$

and

$$\alpha_\nu(k_\parallel,\theta,q,z) = \alpha_\nu\left(k_\parallel, \frac{\pi}{2} - \theta, q, z\right) = \alpha_\nu(k_\parallel, -\theta, q, z) = \alpha_\nu\left(k_\parallel, \frac{\pi}{2} + \theta, q, z\right), \tag{43}$$

and so on.

When the electric field is removed,

$$\overline{\alpha}_\nu \to -\alpha_\nu,$$

$$\overline{\beta}_\nu \to \beta_\nu,$$

and $\psi_\nu^{(0)}$ is degenerate with $\psi_{\overline{\nu}}^{(0)}$. If we neglect the difference between γ_2 and γ_3 in the expression of I, then $\eta = -2\theta$ and the wave function $\psi_\nu^{(0)}$ has in-plane isotropy. Both the $E_\nu^{(0)}$ and $\alpha_\nu(k_\parallel,\theta,z)$ functions become θ independent. This is usually referred to as the axial or cylindrical approximation.

III. SUBBAND STRUCTURES

To quantitatively evaluate the effects of the inversion asymmetry on the subband structure, we have calculated the dispersion curves of a $(\mathrm{GaAs})_{90\ \text{Å}}(\mathrm{AlAs})_{40\ \text{Å}}$ MQW. The parameters used are listed in Table I, most of which are taken or derived from Ref. 23. Parameters, such as $d^{v,cs}$ in Eq. (11) and $d^{v,cp}$ which is related to C_5' in Eq. (18), unavailable from Ref. 23, are taken from pseudopotential calculations reported in Ref. 24. All the $Ga_{1-x}Al_xAs$ parameters are considered identical to those of GaAs except the fundamental gap, which is taken to be $E_g(Ga_{1-x}Al_xAs) = 1.155x + 0.37x^2$. The valence band offset between GaAs and $Ga_{1-x}Al_xAs$ is taken to be 40% of their band-gap difference. No adjustable parameters are used in our calculations. In deriving some of the parameters we need to sum over all intermediate states of the second set. For simplicity, we only included the Γ_{15}^c states. For example, in deriving the parameter B, we assume

$$B \approx 2P'Q\frac{1}{2}\left\{\frac{1}{E_0' - E_g} + \frac{1}{E_0'}\right\}.$$

TABLE I. The parameters used in the multiband $\mathbf{k}\cdot\mathbf{p}$ Hamiltonian for GaAs.

E_g (eV)	$\Gamma_6^c - \Gamma_8^v$	1.519
Δ (eV)	$\Gamma_8^v - \Gamma_7^v$	0.341
E_0' (eV)	$\Gamma_7^c - \Gamma_8^v$	4.488
Δ_0' (eV)	$\Gamma_8^c - \Gamma_7^c$	0.171
P (eV Å)	$i\frac{\hbar}{m_0}\langle X\|p_x\|S\rangle$	10.493
P' (eV Å)	$i\frac{\hbar}{m_0}\langle \Gamma_{15,X}^c\|p_x\|S\rangle$	4.78
Q (eV Å)	$i\frac{\hbar}{m_0}\langle X\|p_y\|\Gamma_{15,Z}^c\rangle$	8.165
γ_1		6.85
γ_2		2.10
γ_3		2.90
m^*		0.0665
a_0 (Å)	lattice const.	5.65
d_{14} (10^{-10} cm/V)	piezoelectric const.	-2.7
C (meV Å)		-3.4
R (Å)	Rashba term	6.91
B (eV Å^2)		21.84
B' (Å^2)		3.53
d (eV)	valence deformation potential	-4.5
C_2 (eV)	$2\sqrt{3}d^{v,cs}$	1.9
C_5 (eV)	calculated from Eqs. (19) and (33)	-8.77

Of course, this will bring in some errors but they are not very significant.

It is well known that the Kramers degeneracy requires a state $(\mathbf{k},\uparrow)$ to have the same energy as another state $(-\mathbf{k},\downarrow)$ in solids. If the crystal potential has inversion symmetry, then the Schrödinger equation is identical for a pair of wave functions $\phi(\mathbf{k},-\mathbf{r})$ and $\phi(-\mathbf{k},\mathbf{r})$, which in general are not eigenstates of the inversion operator, and every energy level is doubly degenerate at a general $\mathbf{k}$ point.[25] This twofold degeneracy is referred to as the spin degeneracy in this paper; it is not the same as the Kramers degeneracy. When there is no inversion symmetry in the potential, the Kramers degeneracy is retained, while the twofold spin degeneracy at a general $\mathbf{k}$ point may be lifted. This spin splitting is the direct consequence of the inversion-asymmetry effects.[26] As estimated in Ref. 4 such a spin splitting for bulk III-V compound semiconductors is less than 0.25 meV.

A. Results for conduction subband

Figure 1 shows the θ dependence of the energy for the first two conduction subbands (CB1) and (CB2) at $k_{\|} = 0.5\frac{2\pi}{L}$ for the $(\mathrm{GaAs})_{90\ \text{Å}}(\mathrm{AlAs})_{40\ \text{Å}}$ MQW with $F = 3.65\times10^4$ V/cm. Here the solid and dotted lines represent the anisotropic dispersion curves with and without taking into account the Rashba term, respectively. Here we still follow the usual nomenclature, referring the pair of spin splitting states to their doubly degenerate sub-

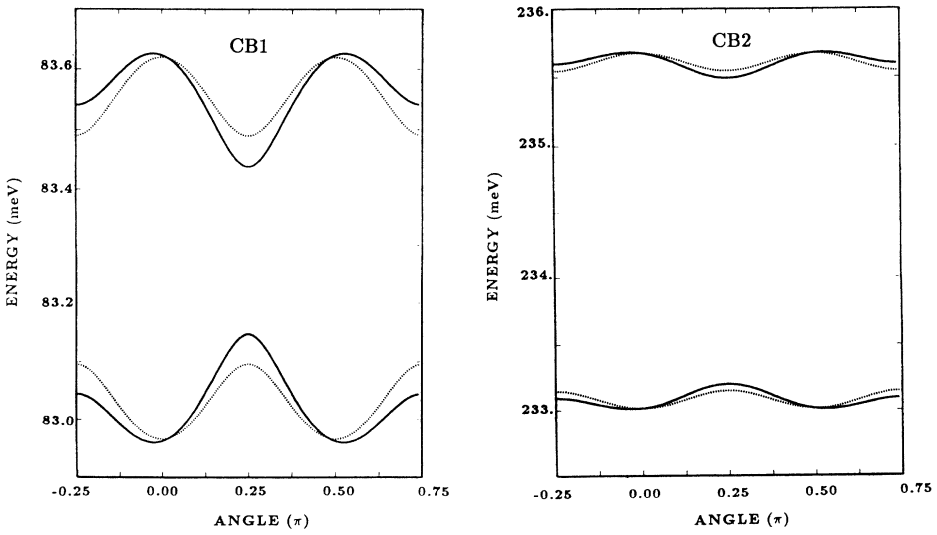

FIG. 1. Angular dependence of the CB1 and CB2 energy at $k_{\|} = 0.5\frac{2\pi}{L}$ for the $(\mathrm{GaAs})_{90\ \text{Å}}(\mathrm{AlAs})_{40\ \text{Å}}$ MQW in an electric field of 3.65×10^4 V/cm. Solid lines: with the Rashba term; dotted lines: without the Rashba term.

band at the zone center. If not necessary, we do not distinguish them.

It is evident from Fig. 1 that the inversion asymmetry breaks the fourfold rotational symmetry. Generally speaking, $E(\theta) \neq E(\frac{\pi}{2}+\theta)$ and $E(\theta) \neq E(-\theta)$. However, not all the symmetry properties are broken; in addition to twofold rotational symmetry, $E(\theta) = E(\pi+\theta)$, there exists reflection symmetry about $\theta = \frac{\pi}{4}$, i.e., $E(\theta) = E(\frac{\pi}{2}-\theta)$. Such symmetry properties can also be proved by analyzing the angular dependence of Eq. (24), and they remain correct when the Rashba term is included. Thus we can study the angular dependence of the subband from the region of $\theta \in (-\frac{\pi}{4}, \frac{\pi}{4})$. By this symmetry it can be inferred that the spin splittings along [100] and [010] are always the same, while the difference between any other two mutually perpendicular directions is nonzero.

In addition to the symmetry, there are several other characteristics of the in-plane anisotropic conduction subband. First, as demonstrated in Fig. 1, the spin splitting can be decomposed into an angular independent (isotropic) and an angular dependent (anisotropic) part. For both subbands, the isotropic part dominates the anisotropic part, and the isotropic part of CB2 is much larger than that of CB1. The amplitudes of the anisotropic part of both subbands are roughly the same, and they increase with the in-plane wave number. Second, the Rashba term significantly increases the anisotropy between $[1\bar{1}0]$ and [110] directions. For $k_{\|} = 0.5\frac{2\pi}{L}$ and without the Rashba term, as shown by Fig. 1, both the CB1 and CB2 states have the largest spin splitting along the [100] or [010] direction; while the smallest splitting occurs at around either $\theta = \frac{\pi}{4}$ (along [110]) or $\theta = -\frac{\pi}{4}$ (along $[1\bar{1}0]$), depending on the wave number. When the Rashba term turns on, the difference between spin splittings along [110] and $[1\bar{1}0]$ directions becomes evident. For large $k_{\|}$, the largest spin splitting is still around the [100] or [010] direction. For small $k_{\|}$, however, since the product of the Rashba term and $C_2\epsilon$ in Eq. (24) becomes dominant for the angular dependent part, the largest splitting may occur at $\theta = -\frac{\pi}{4}$ while the smallest splitting is still around $\theta = \frac{\pi}{4}$. Third, when the wave number $k_{\|}$ increased, the spin splitting increases too.

If we assume an effective k_z for the μth subband wave function to be about $\mu\frac{\pi}{W}$, then all the characteristics above can be explained qualitatively by inserting this effective k_z into Eq. (24). Clearly, due to the relatively large effective k_z selected by the quantum well, the term containing $k_z^2k^2$ in Eq. (24) makes the largest contribution to the isotropic spin splitting, and the term $-k_{\|}^2k_z^2(1-\cos 4\theta)$ is the main factor for the anisotropy provided that $k_{\|}$ is not too small.

We have also evaluated the energy minimum shift by the linear k term. For the $(GaAs)_{90\ \text{Å}}(AlAs)_{40\ \text{Å}}$ MQW with $F = 3.65\times10^4$ V/cm, we found that the wave number associated with the energy minimum is about $0.003\frac{2\pi}{L}$ for CB1 and $0.01\frac{2\pi}{L}$ for CB2. The energy reduction due to the linear k term is about 0.001 meV for CB1 and 0.014 meV for CB2.

The spin splitting is not sensitive to the electric field. For example, for the case above, when the field strength is doubled, the splitting of CB1 is enhanced while that of CB2 is reduced. The relative variation is only about 1%.

B. Results for hole subbands

The spin splitting and anisotropic in-plane energy dispersion for the hole subbands have the same symmetry properties as those for the electrons. Furthermore, some qualitative characteristics of the anisotropy for the electrons are kept with some revisions.

Let us define

$$u_{\nu,\nu'} = \langle\psi_{\nu}^{(0)}|\mathbf{H}_h^{(1)}|\psi_{\nu'}^{(0)}\rangle, \tag{44}$$

$$u_{\bar{\nu},\bar{\nu}'} = \langle\psi_{\bar{\nu}}^{(0)}|\mathbf{H}_h^{(1)}|\psi_{\bar{\nu}'}^{(0)}\rangle, \tag{45}$$

$$w_{\bar{\nu},\nu'} = \langle\psi_{\bar{\nu}}^{(0)}|\mathbf{H}_h^{(1)}|\psi_{\nu'}^{(0)}\rangle, \tag{46}$$

and

$$w_{\nu,\bar{\nu}'} = \langle\psi_{\nu}^{(0)}|\mathbf{H}_h^{(1)}|\psi_{\bar{\nu}'}^{(0)}\rangle. \tag{47}$$

In addition to the twofold rotational invariance, these matrix elements of the inversion-asymmetry Hamiltonian have the following symmetry:

$$u(\theta) = u\left(\frac{\pi}{2}-\theta\right) \tag{48}$$

and

$$w(\theta) = -w\left(\frac{\pi}{2}-\theta\right) \tag{49}$$

with the subscripts kept implicit. We shall not give the explicit expressions for these u and w functions. It should be pointed out that u denotes the coupling by the inversion-asymmetry Hamiltonian between the hole states of the same symmetry, the most important one being its first-order perturbation energy, while w denotes the coupling between the states of opposite symmetry with the main contribution coming from the coupling between a pair of spin splitting states or states close in energy. One interesting point is that, for states at $\theta = 0$ or $\pi/2$, the first-order correction in energy is very small (only the terms $C_5\epsilon k_{\|}$ and $Ck_{\|}$ have nonvanishing contributions), but, owing to contributions from the intersubband coupling and the intrasubband w, the final splitting is quite comparable to that at $\theta = \pm\pi/4$. Another point easy to deduce from Eq. (49) is that $w(\theta = \pm\pi/4) = 0$.

Since there is in-plane reflection symmetry with respect to $[1\bar{1}0]$ and [110] in hole subbands, the expansion coefficients $b_{\nu,\nu'}$ and $b_{\bar{\nu},\bar{\nu}'}$ in Eq. (37) will possess the same symmetry properties with the matrix elements u, while $b_{\nu,\bar{\nu}'}$ and $b_{\bar{\nu},\nu'}$ will behave like w. This determines why the polarization ratio of these two mutually perpendicular directions of [100] and [010] is zero.

There are several factors qualitatively affecting the hole spin splitting and in-plane anisotropy compared to the electrons. First, unlike the conduction subbands which are degenerate in the presence of the electric field

without inversion asymmetry, the twofold degeneracy of the hole subbands is lifted in the electric field even if the inversion-asymmetry term is omitted (i.e., $\mathbf{H}_h^{(1)} = 0$), because the electric potential breaks the spin degeneracy via the spin-orbit coupling in the valence band. The dotted lines in Fig. 2 represent the angular variation of the first four hole subbands in a field without taking the inversion asymmetry into account. The splitting of these dotted lines is significant, and, as indicated by our calculations, it increases considerably with the field strength. So the total spin splitting for holes results from both the inversion asymmetry and the applied field. It is worth noticing that the spin splitting caused by the electric field has fourfold rotational symmetry, if inversion symmetry exists.

Second, even without the inversion asymmetry and the electric field, the in-plane dispersion for the hole subbands is anisotropic. In other words, there is in-plane warping for the hole energy spectrum (see dotted lines in Fig. 2). So the total anisotropic part of the in-plane dispersion is the sum of the warping as well as the lack of inversion symmetry. This is why the anisotropic part of the hole spin splitting dominates over the isotropic part (see Fig. 2) which seems in sharp contrast to the result for the electrons, but if we eliminate the contribution due to warping, the difference is not so great.

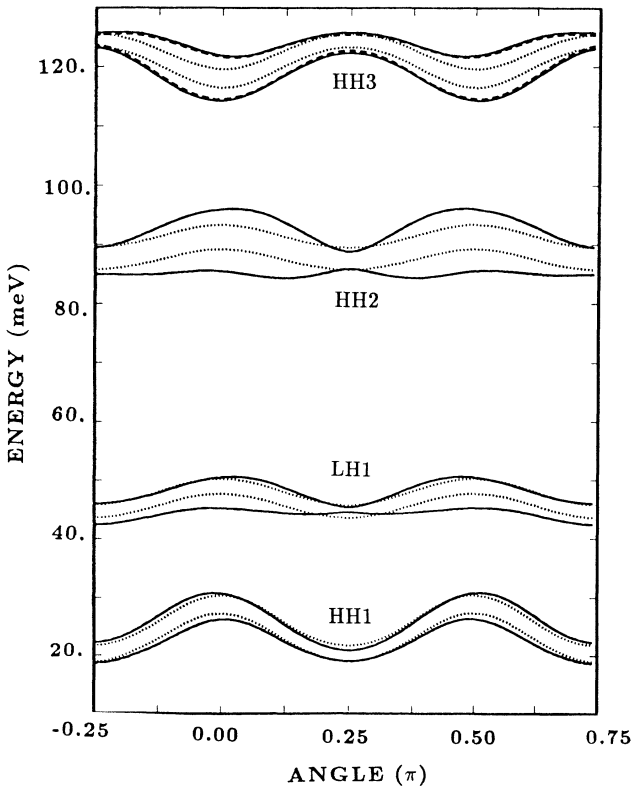

FIG. 2. Angular dependence of the four lowest hole subbands at $k_{\|} = 1.0\frac{2\pi}{L}$ for the $(GaAs)_{90\ \text{Å}}(AlAs)_{40\ \text{Å}}$ MQW in an electric field of 3.65×10^4 V/cm. Dotted lines: without inversion asymmetry; dashed lines: with inversion asymmetry but without the Rashba term; solid lines: with everything.

Third, there is a heavy-hole (HH) and light-hole (LH) mixing effect in MQW's and SL's, which is lacking for conduction subbands. The meaning of HH and LH mixing is twofold. On the one hand, the nondiagonal matrix elements of the hole Hamiltonian lead to strong admixture of the $\pm 3/2$ and $\pm 1/2$ components of the Γ_8^v representation in the subband states at sufficiently large $k_{\|}$, which is viewed as hole mixing in the subbands. On the other hand, due to different in-plane curvatures, different hole subbands tend to cross each other at finite $k_{\|}$. Near the crossing region, two subbands can mix heavily. The hole mixing and the inversion-asymmetry Hamiltonian $\mathbf{H}_h^{(1)}$ are interdependent, the latter will cause coupling between different subbands, and certainly, the hole mixing will affect the spin splitting of the hole states in quantum wells.

Figure 3 shows the calculated hole dispersion curves along (a) [100], (b) [110], and (c) [1$\bar{1}$0]. It is interesting to compare Fig. 3(b) with Fig. 3(c), which clearly shows the opposite role played by the inversion asymmetry along [110] and [1$\bar{1}$0]. When the inversion asymmetry increases the splitting along one direction, it decreases the splitting along the other direction, and vice versa. Since the dispersion curves represented by the dotted lines along these two directions are the same, such an opposite change along the two directions means that *the inversion asymmetry produces the anisotropy between* [1$\bar{1}$0] *and* [110]. On the other hand, the dispersion curves along [100] and [010] are exactly the same, which means these two directions are equivalent as far as the inversion asymmetry is concerned. Figure 3 indicates that, when two subbands undergo "subband crossing," the relative change in spin splitting along [1$\bar{1}$0] and [110] manifests itself more considerably.

Let us take a close look at Figs. 1–3. There are still some important quantitative differences in the behavior of the anisotropy and splitting between the hole and the electron in the following aspects.

(1) Even subtracting the splitting contributed by the electric field from the total splitting, and subtracting the anisotropic warping effects from the total anisotropic part, the splitting as well as the anisotropy of splitting in hole subbands is still much larger than the corresponding one in the electron subbands. Comparing U' in Eq. (23) with U in Eq. (31), the most important source for spin splitting and anisotropy in MQW's, we found that there is a factor $\frac{\Delta}{\Delta+E_g}$ in Eq. (23), which equals 0.183 in GaAs. That is why the spin splitting and anisotropy in holes is more significant than for the electrons.

(2) Due to the hole mixing, warping, and the field-induced splitting, the angular dependence of the hole spin splitting becomes more complicated; it not only depends on $k_{\|}$ but also on the subband index, on the field strength, and on the MQW structure parameters. For a moderate field strength the maximum spin splitting in HH1 (the first heavy-hole subband) of the $(GaAs)_{90\ \text{Å}}(AlAs)_{40\ \text{Å}}$ MQW is at around $\theta = \frac{\pi}{4}$ for $k_{\|} \leq 0.5\frac{2\pi}{L}$ and gradually changes to the neighborhood of $\theta = 0$ or $\pi/2$ when the wave number increases.

(3) Although the Rashba term is also increased by a

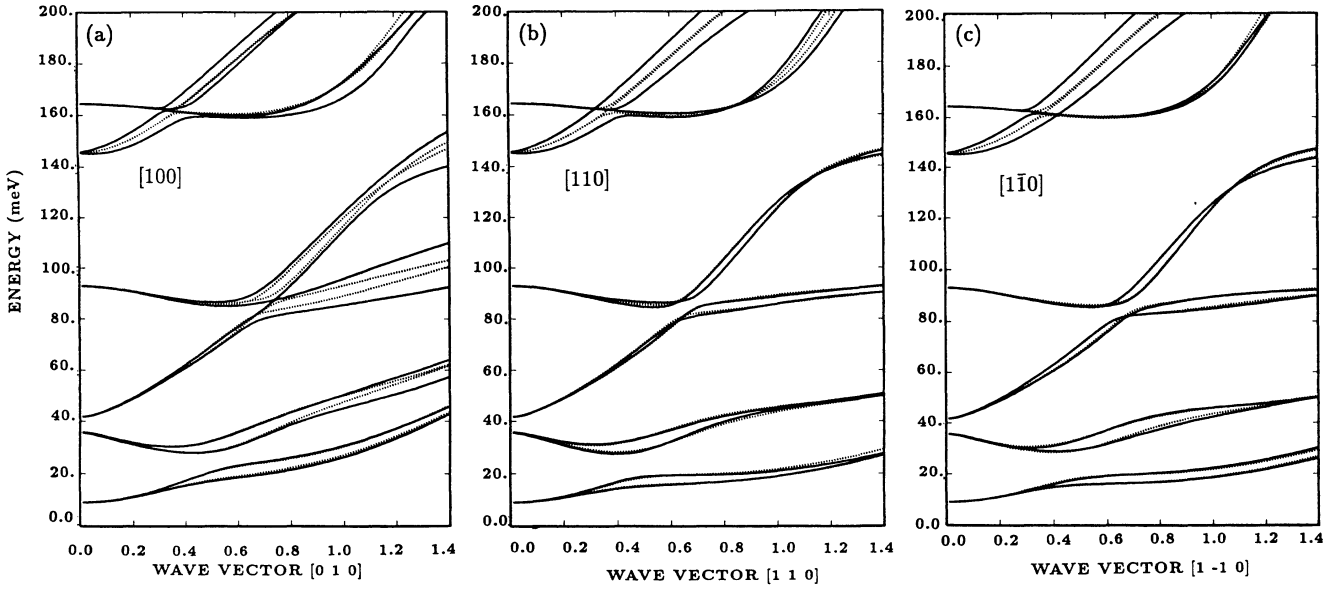

FIG. 3. Hole subband dispersion curves along three specific directions ([100], [110], and [1$\bar{1}$0]) for $(GaAs)_{90\ \text{Å}}(AlAs)_{40\ \text{Å}}$ MQW in an electric field of 3.65×10^4 V/cm. Solid lines: with inversion asymmetry; dotted lines: without inversion asymmetry.

factor of $\frac{\Delta+E_g}{\Delta}$ in the hole inversion-asymmetry Hamiltonian, its contribution is relatively small and only important for situations where there are no competitors, as is the case for the electron spin splitting. Since many competing factors affect the hole splitting significantly, the Rashba term plays a relatively minor role in the hole spin splitting.

Besides, although the hole spin splitting enlarges with increasing $k_{\|}$ on average, owing to the hole mixing effect, it does not always monotonically increase like the electron spin splitting does.

IV. INTERBAND OPTICAL TRANSITIONS

The interband optical transition can be written as:

$$O(\hbar\omega) \propto \frac{1}{\omega} \sum_{\mu\nu} \sum_{\mathbf{k}} |\langle \phi_\mu | \hat{\varepsilon} \cdot \mathbf{p} | \psi_\nu \rangle|^2 \delta(\hbar\omega - E_\mu - E_\nu), \tag{50}$$

where $\hat{\varepsilon}$ is the polarization unit vector of the light with frequency ω. Assuming the momentum matrix element $\overline{P}$ is independent of the wave vector, following the common practice in SL's and MQW's, the optical transition matrix element above is transformed to an overlap integral between each component of the electron and hole envelope functions over the z axis multiplied by a corresponding band-edge matrix element. Here, the electron state ϕ_μ is a spinor associated with two components,

$$\phi_\mu(\mathbf{k}_e) \equiv \exp[i\mathbf{k}_{\|} \cdot \rho_e + iqz_e] \begin{pmatrix} f_{\mu,\uparrow}(\mathbf{k}_e) \\ f_{\mu,\downarrow}(\mathbf{k}_e) e^{i\theta} \end{pmatrix}, \tag{51}$$

and its nearly degenerate partner is

$$\phi_{\bar{\mu}}(\mathbf{k}_e) \equiv \exp[i\mathbf{k}_{\|} \cdot \rho_e + iqz_e] \begin{pmatrix} -\overline{f}_{\mu,\uparrow}(\mathbf{k}_e) \\ \overline{f}_{\mu,\downarrow}(\mathbf{k}_e) e^{i\theta} \end{pmatrix}. \tag{52}$$

The hole state ψ_ν is defined in Eq. (37).

We define the polarization ratio between the [100] and [010] directions at frequency ω as

$$P_{xy}(\omega) = \frac{O_{[100]} - O_{[010]}}{O_{[100]} + O_{[010]}}$$

and that between [1$\bar{1}$0] and [110] as

$$P_{x'y'}(\omega) = \frac{O_{[1\bar{1}0]} - O_{[110]}}{O_{[1\bar{1}0]} + O_{[110]}}.$$

Since the system (a superlattice made of zinc-blende materials) is invariant under a reflection about a plane containing the [001] and [110] axes (i.e., exchanging x and y), we must have $O_{[100]} = O_{[010]}$ and therefore $P_{xy} = 0$. However, $O_{[1\bar{1}0]}$ and $O_{[110]}$ do not have to be the same; thus $P_{x'y'}$ is in general nonzero. Furthermore, the system is invariant under a fourfold rotation followed by inversion (i.e., $x \to -y, y \to x$, and $z \to -z$); therefore the reversal of the electric field would result in the exchange of $O_{[1\bar{1}0]}$ and $O_{[110]}$, which means that $P_{x'y'}$ is an odd function of the electric field.

Figure 4 shows the angular dependence of the optical transition strengths for a pair of electron and hole subbands at a given $k_{\|}$ with the polarization vector of the incident light parallel to [100], [010], [1$\bar{1}$0], or [110]. For each curve, we have added up four optical transition probabilities between two nearly degenerate electrons and two nearly degenerate holes. Note that the angular distribution is symmetric about $\theta = \pi/4$ for the [1$\bar{1}$0] and [110] polarizations, and these two curves have quite different amplitudes. On the other hand, for the [100] and [010] polarizations, there is no such symmetry

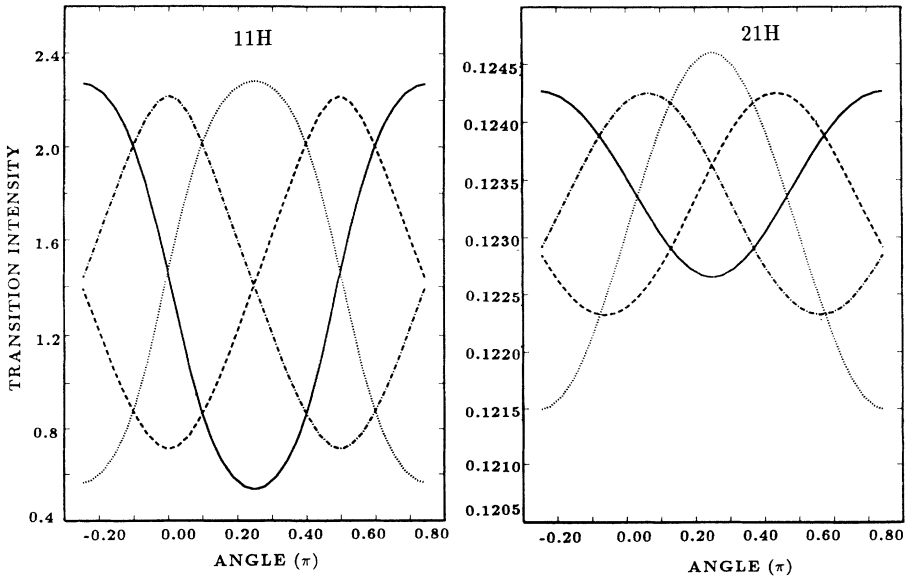

FIG. 4. Angular dependence of the 11H and 21H interband transition strengths at $k_{\|} = 0.1\frac{2\pi}{L}$ for a $(GaAs)_{90\ \text{Å}}(AlAs)_{40\ \text{Å}}$ MQW in an electric field of 3.65×10^4 V/cm. Four different polarizations are shown, dotted: $[1\bar{1}0]$; solid: [110]; dashed: [100]; dash-dotted: [010].

for each curve; while these two curves are mirror reflections of each other about $\theta = \pi/4$. This is consistent with the above conclusion that the polarization ratio between [100] and [010] is zero.

Compared with the "allowed transition" of CB1-HH1 (11H) at the wave number $k_{\|} = 0.1\frac{2\pi}{L}$ [Fig. 4(a)], the "forbidden transition" between CB2-HH1 (21H) at the same wave number exhibits larger difference in amplitude between the $[1\bar{1}0]$ and [110] polarizations [Fig. 4(b)]. Significant differences in amplitude are also observed at several other transitions associated with certain $k_{\|}$, especially those at "subband crossings," e.g., $k_{\|} = 0.5\frac{2\pi}{L}$ for 11L and 21L transitions, and $k_{\|} = 0.7\frac{2\pi}{L}$ for 12H and 22H transitions, etc.

According to Eq. (50) we have calculated the polarization-dependent absorption spectra of the MQW $(GaAs)_{90\ \text{Å}}(AlAs)_{40\ \text{Å}}$ in the presence of an electric field. The results for $[1\bar{1}0]$ and [110] polarizations are shown in Fig. 5 for (a) $F = 3.65 \times 10^4$ V/cm and (b) $F = 1.1 \times 10^5$ V/cm. Two conduction subbands and twelve valence subbands are included in this calculation.[27] A Lorentzian function with a half-width at half-maximum of 0.5 meV is used to simulate the δ function in Eq. (50). 600 $k_{\|}$ points, 10 q points, and 10 θ points ranging from $-\pi/4$ to $\pi/4$ for each transition are used. In addition to the total absorption we have also calculated the individual contributions from different subband-subband transitions.

Figure 6 shows the calculated polarization ratio $P_{x'y'}$ for the interband transitions discussed above. The polarization ratios due to individual subband transitions are also shown in the same figure. Several points are worth mentioning.

(1) Although the total polarization ratio is small, it is enhanced greatly compared to the bulk result. In particular, at certain frequencies (e.g., near the 11L absorption peak, which results from the negative mass of the light hole near the band center) the total $P_{x'y'}$ is beyond 5% for the field strength of 1.1×10^5 V/cm, about 3% for

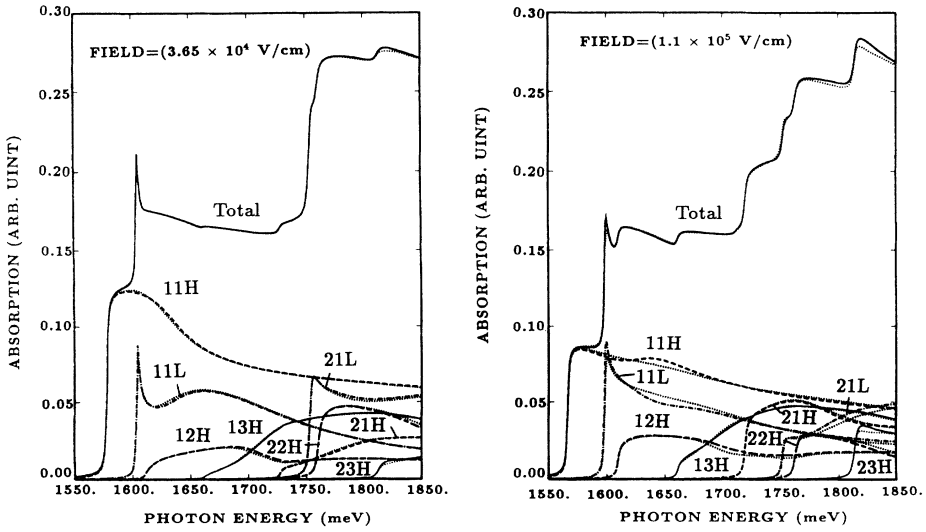

FIG. 5. Interband absorption spectra of the $(GaAs)_{90\ \text{Å}}(AlAs)_{40\ \text{Å}}$ MQW under two different electric fields: 3.65×10^4 V/cm and 1.1×10^5 V/cm. Contributions from individual pairs of subbands are labeled. Solid, dashed, and dash-dotted lines are for the $[1\bar{1}0]$ polarization, while the dotted lines are for the [110] polarization.

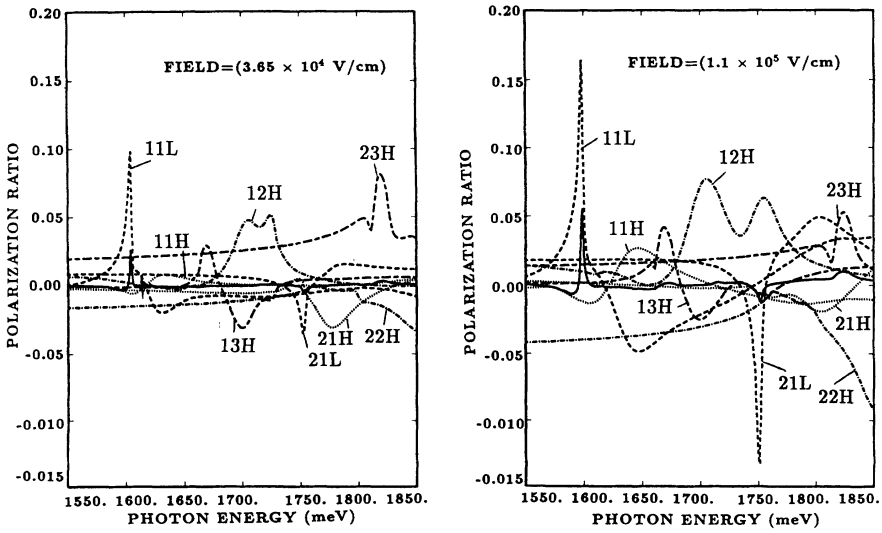

FIG. 6. Polarization ratio as a function of photon energy for the $(GaAs)_{90\,\text{Å}}$-$(AlAs)_{40\,\text{Å}}$ MQW under two different electric fields: 3.65×10^4 V/cm and 1.1×10^5 V/cm. Contributions from individual pairs of subbands are labeled. Solid lines are for the total contribution.

$F = 3.65 \times 10^4$ V/cm, and 1% near the 21L absorption edge. As for polarization ratio due to each subband, the enhancement is more impressive. The extent of the polarization ratio of 11L varies from 17 (10)% to -5 (-3)% and that of 21L is as large as 5 (3)% to -13 (3)% in the field of 1.1 (0.365) $\times 10^5$ V/cm. For other subbands, the maximum value of the 12H transition is as large as 8 (5) % and of the 21H transition as -2 (-3) % in the field of 1.1 (0.365) $\times 10^5$ V/cm, respectively.

(2) Figure 6 shows that the polarization ratios, especially those due to individual subband-subband transitions, have a substantial variation with the light frequency. Such frequency dependence of the polarization ratio in fact reflects the variation of $P_{x',y'}$ with the wave vector of the electron-hole pair. With different $k_{\|}$, the matrix elements of the inversion-asymmetry Hamiltonian vary a lot. For example, when the wave number is less than $0.6\frac{2\pi}{L}$, the coupling coefficients between the HH2 and HH3 subbands are at most about 0.02 for the sample in the field of 3.65×10^4 V/cm; but when wave number is around $0.7\frac{2\pi}{L}$, the intersubband coupling coefficient is as large as 0.5. This means that the inversion asymmetry Hamiltonian leads to something like a " resonance coupling" between these two subbands. Because of the spin splitting, two spin-split states belonging to a subband will couple with another two spin-split states differently, which will certainly influence the polarization ratio. In addition to the intersubband coupling, the inversion-asymmetry Hamiltonian also causes intrasubband coupling, for those states which contain admixtures of heavy- and light-hole states, a subtle change will result in a significant change in the polarization ratio, e.g., the 11L transition at $k_{\|} = 0.5\frac{2\pi}{L}$.

(3) On average the polarization ratio for interband transitions is increased when the field increases. However, there are exceptions. For example, the 21H transition has a larger $P_{x'y'}$ in a weaker field than in a stronger field, as indicated above.

(4) Neglecting the q dependence of the subband structure, i.e., assuming all the subband states have zero superlattice wave number along the z direction, gives essentially the same results as those obtained by including the q dependence.

(5) Although for some "forbidden transitions" the polarization ratio between $[1\bar{1}0]$ and [110] looks significant, its absolute strength is relatively small, so it hardly makes any contribution to the total polarization ratio.

V. EFFECTS OF INVERSION ASYMMETRY ON EXCITON STRUCTURE AND ITS OPTICAL TRANSITION

A. Formalism

Owing to the spatial confinement, the quasi-two-dimensional exciton state plays a special role in MQW optical processes. Usually the hole state from the valence band of Γ_8^v symmetry is a spinor of four components. Hence the exciton state is also a spinor of four components (ignoring the electron spin) in the absence of inversion asymmetry. It has been shown that out of the four components for an exciton state only one component can contribute to the optical transition; this can be referred to as the optically active component of the exciton state.[21,28–31] We can also prove that, in the electric field and with the warping effect of the hole included, it is still true that only one component of an exciton state makes a contribution to the optical transition. It is easy to verify that, if only one component of an exciton state contributes to the optical transition, both P_{xy} and $P_{x'y'}$ vanish despite the presence of electric field and warping. This means that the excitonic Pockels effects critically depend on the interference between the several optically active components.

When the inversion asymmetry is included, the nondegenerate Γ_6^c subband electron has two components [Eqs. (51) and (52)], corresponding to spin-up and spin-down components. Thus, in general, an exciton state is a spinor of eight components, and can be expressed as summation of several two-subband exciton states associated with the same phase factor. The two-subband exciton state derived from the μth conduction subband and νth valence subband is in turn a linear combination of two spin-split electron states and two spin-split hole states, because the

exciton binding energy is usually much larger than the spin splitting energy.

Since the phase factor in the exciton spinor determines which component is the optically active component, in the following we add another index to designate the component whose phase factor equals 1. For example, $\frac{1}{2}$ $(-\frac{1}{2})$ indicates that the $\uparrow$ $(\downarrow)$ component phase factor in Eq. (51) or (52) is 1; and m_j $(m_j = \pm\frac{3}{2}, \pm\frac{1}{2})$ indicates that the phase factor in the m_j component of the valence electron state in Eq. (39) or (40) is 1. Thus, one of the $\mu'\nu'$ HH $1s$-state excitons which may emit a photon with $M_z = -1$ can be expanded in terms of several exciton terms, including the $2p$ state of the neighboring subbands,

$$|\mathrm{ex}, \mu'\nu' H, 1s, -1\rangle = \sum_{\mu\nu} \sum_{\mathbf{k}_\parallel, q} G^{nm}_{\mu,\nu}(\mathbf{k}_\parallel)\{g_1^{\mu\nu}\phi^{\frac{1}{2}}_{\mu}(\mathbf{k}_\parallel, q)\hat{K}[\psi^{\frac{3}{2}}_{\nu}(\mathbf{k}_\parallel, q)] + g_2^{\mu\nu}\phi^{\frac{1}{2}}_{\mu}(\mathbf{k}_\parallel, q)\hat{K}[\psi^{\frac{3}{2}}_{\nu}(\mathbf{k}_\parallel, q)]$$
$$+ g_3^{\mu\nu}\phi^{\frac{1}{2}}_{\mu}(\mathbf{k}_\parallel, q)\hat{K}[\psi^{\frac{3}{2}}_{\nu}(\mathbf{k}_\parallel, q)] + g_4^{\mu\nu}\phi^{\frac{1}{2}}_{\mu}(\mathbf{k}_\parallel, q)\hat{K}[\psi^{\frac{3}{2}}_{\nu}(\mathbf{k}_\parallel, q)]\}. \tag{53}$$

Here the operator $\hat{K}$ represents the time reversal operator, and $g_i^{\mu\nu}$ are the expansion coefficients which will be determined later by solving a generalized secular equation. $G^{nm}_{\mu,\nu}(\mathbf{k}_\parallel)$ is the exciton correlation function in momentum space. The Fourier-transformed two-dimensional hydrogenlike orbitals are written as

$$G^{1s} = \sqrt{2\pi}\frac{2\zeta^2}{(\zeta^2 + k_\parallel^2)^{\frac{3}{2}}},$$

$$G^{2s} = \sqrt{2\pi}\frac{2\sqrt{3}\zeta^2(k_\parallel^2 - \zeta^2)}{(\zeta^2 + k_\parallel^2)^{\frac{5}{2}}},$$

$$G^{2p\pm} = \sqrt{2\pi}e^{i\pm\theta}\frac{2\sqrt{6}\zeta^3 k_\parallel}{(\zeta^2 + k_\parallel^2)^{\frac{5}{2}}},$$

$$G^{3d\pm} = \sqrt{2\pi}e^{i\pm 2\theta}\frac{2\sqrt{30}\zeta^4 k_\parallel^2}{(\zeta^2 + k_\parallel^2)^{\frac{7}{2}}},$$

where ζ is a variational parameter. In the calculation, we take several different ζ parameters to cover a wide range of $k_\parallel$; thus the total dimension of the exciton matrix is the sum of the terms in Eq. (53) multiplied by the number of ζ for each term. In principle, there is no difficulty in solving the exciton problem, so we will not detail all the formulas. The differences between the present work and previous work[28] are solely numerical. Not only is the number of the basis functions quadrupled here, the integration over θ and the choice of the phase factors in constructing the exciton wave function in k space are more time consuming. A large amount of computation is needed for the calculation of the Coulomb matrix elements between two exciton terms, which is carried out by expanding in terms of the plane waves.[10,30]

One important question about the quantum well excitonic optical transition is how many components are responsible for the excitonic optical transition? Let us first analyze an optical transition matrix element using an exciton term taken from Eq. (53).

$$\langle \mathrm{ex}|\hat{\varepsilon}\cdot\mathbf{p}|0\rangle = \sum_{k_\parallel\theta} G^*(k_\parallel)\langle\phi^{\frac{1}{2}}_{\mu}(\mathbf{k}_\parallel, q)|\hat{\varepsilon}\cdot\mathbf{p}|\psi^{\frac{3}{2}}_{\nu}(\mathbf{k}_\parallel, q)\rangle$$
$$= \int dz \sum_{k_\parallel\theta} G^*(k_\parallel)[f^*_{\mu,\uparrow}(k_\parallel, \theta, q)\langle S\uparrow| + f^*_{\mu,\downarrow}(k_\parallel, \theta, q)e^{-i\theta}\langle S\downarrow|]\hat{\varepsilon}\cdot\mathbf{p}$$
$$\times[\alpha_\nu(k_\parallel, \theta, q, z)|\Gamma_8, \tfrac{3}{2}\rangle + \beta_\nu(k_\parallel, \theta, q, z)e^{i\theta}|\Gamma_8, \tfrac{1}{2}\rangle$$
$$+ i\beta_\nu(k_\parallel, \theta, q, z)e^{-i\eta}|\Gamma_8, -\tfrac{1}{2}\rangle - i\alpha_\nu(k_\parallel, \theta, q, z)e^{i\theta - i\eta}|\Gamma_8, -\tfrac{3}{2}\rangle]. \tag{54}$$

In view of the fact that all the electron and hole envelope functions have twofold rotational symmetry, and when θ is transformed into $\theta + \pi$, both $e^{\pm i\theta}$ and $e^{\pm i(\theta\pm\eta)}$ change sign, so the integral above containing these factors will be zero; this includes the $\langle S\uparrow|\Gamma_8, \frac{1}{2}\rangle$, $\langle S\downarrow|\Gamma_8, \frac{3}{2}\rangle$, $\langle S\uparrow|\Gamma_8, -\frac{3}{2}\rangle$, and $\langle S\downarrow|\Gamma_8, -\frac{1}{2}\rangle$ components. All the other four out of the eight components in principle can contribute to the excitonic optical transition, which is different from the case for the system with an inversion center. For the latter, the electronic states keep the spin degeneracy; thus in effect only four components need considering. Because $e^{i\eta}$ changes sign while the envelope function remains the same under a fourfold rotation, the $e^{i\eta}$ term also has no contribution. Although in fact only one out of the four contributors dominates, owing to the nonvanishing transitions by these excitonic components, the excitonic Pockels effect takes place.

B. Exciton Pockels effects

The exciton Pockels effect in essence is the integration of the interband Pockels effect of a large number of electron-hole pairs weighted by the exciton correlation function in reciprocal space. Usually, the electron-hole pairs near the zone center, being the main components to produce an s-state exciton, contribute more to the s-state exciton Pockels coefficient. The exciton state with stronger binding energy, being more localized

in real space, covers a wider range in the wave vector space. Thus, based on the polarization ratio curves originating from each interband transition as shown in the last section, and on the exciton selection rules as well as the exciton binding, the Pockels effect due to that two-subband exciton can roughly be estimated.

This argument above is true for a general situation, but not totally suitable for the MQW exciton state. Though the subband electron-hole pair polarization optical spectrum has already included some aspects of the hole mixing effects, the hole mixing effect on the exciton itself introduces several additional complicating factors. First, it makes the oscillator strength and the binding energy be not always correlated because the optically active components are not always the dominant components, especially for the p-state excitons.[29] For example, the CB2-LH1 $2p$-state exciton has a dominant component with index of $\pm 1/2$, but, as a p-state exciton, its optically active component is $\pm 3/2$, which becomes possible entirely due to its mixing with the HH2 subband. In the p-state exciton correlation function, the weight factor of small $k_{\|}$ is small; thus it will not be easy to evaluate the exciton Pockels effect from the electron-hole pair curves. Moreover, owing to hole mixing, the polarization ratio of a pair subband varies significantly with the wave number, which makes it even more difficult to predict the average behavior of an exciton state. Second, because of the narrow energy separation in the MQW subband structure, the Coulomb interaction will couple several different two-subband exciton states. Although some gain oscillator strength at the expense of the others, it occurs at different energy, hence giving rise to rich structure. Furthermore, the polarization ratio describes the difference of the oscillator strengths along two perpendicular directions; it is hard to know the change in $P_{x'y'}$ due to the Coulomb coupling of the two-subband excitons without calculations.

Figure 7 shows the calculated oscillator strengths versus the electric field for three exciton states: 21H $1s$, 21L $2p$, and 22H $1s$ with the Coulomb coupling between two-subband excitons included (left panel) or excluded (right panel). We found that the Coulomb-induced exciton coupling results in considerable changes in the oscillator strengths, especially the increased oscillator strength for the 21L $2p$ exciton and the decreased one for the 22H $1s$ exciton. However, in the polarization ratio spectrum, there is little change due to the exciton coupling for the 21L $2p$ exciton, but a remarkable change for the 22H $1s$ exciton as shown in Fig. 8 below.

Figure 8 shows the polarization ratios versus the field for the above three excitons. Note that because of the different conventions used in this paper and Ref. 1, the polarization ratio $P_{x'y'}$ defined here as the difference between $[1\bar{1}0]$ and [110] polarizations corresponds to the quantity $I_{\|}^{-}$ (i.e., the difference of the oscillator strengths between [110] and $[1\bar{1}0]$ polarizations) defined in Ref. 1. The 21H $1s$ exciton [Fig. 8(a)] is dipole forbidden without the electric field, because the envelope function for the optically active component of HH1 is an even function of z and that of CB2 is odd. The electric field relaxes the parity requirements on the envelope functions; thus the exciton has a finite oscillator strength. At a weak field, the optical transition matrix element of the optically active component is small, comparable to other components which become allowed entirely due to the inversion asymmetry and are favored by the parity. Thus, the interference between them makes the polarization ratio maximum be as large as 60% at very low field, though both have very small oscillator strengths. With the field increased, the 21H $1s$ state gains oscillator strength but loses anisotropic character.

Owing to the strong heavy-hole and light-hole mixing at small $k_{\|}$, the LH1 exciton state has attracted special attention. The 21L $2p$ exciton is dipole allowed even without the electric field because the envelope function of its optically active component (3/2), heavily hybridized with HH2, is an odd function of z, matched with that

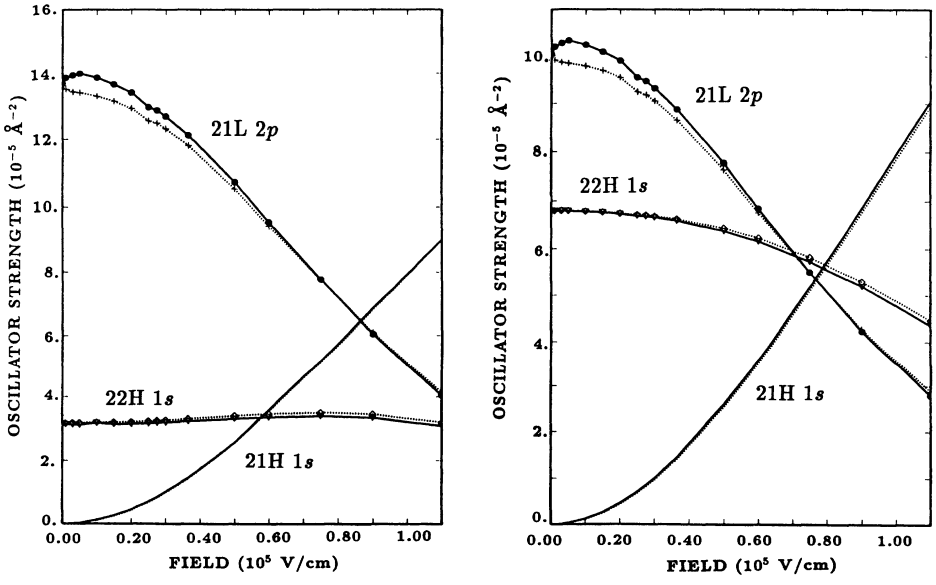

FIG. 7. Oscillator strengths for 21H $1s$, 21L $2p$, and 22H $1s$ exciton states of the $(GaAs)_{90\ \text{Å}}(AlAs)_{40\ \text{Å}}$ MQW as functions of the electric field. Solid lines: $[1\bar{1}0]$ polarization; dotted lines: [110] polarization. The Coulomb coupling between two-subband excitons is included in the left panel and excluded in the right panel.

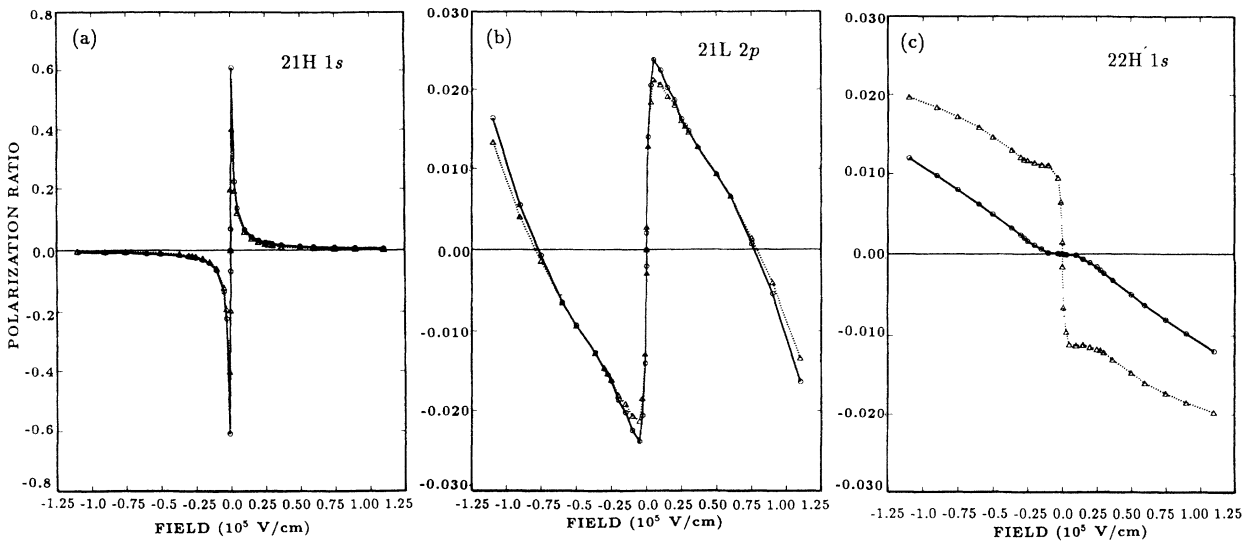

FIG. 8. Polarization ratio versus the electric field for 21H 1s, 21L 2p, and 22H 1s exciton states of the $(GaAs)_{90\,\text{Å}}(AlAs)_{40\,\text{Å}}$ MQW. The solid lines and dotted lines stand for the polarization ratios without and with the coupling between different two-subband excitons, respectively.

of CB2. Since both the dominant component (1/2), an even function in the absence of the field, and the optically active one (3/2) are significant, this exciton has a really observable effect in the polarization spectrum (see Fig. 7). An interesting point in its polarization spectrum is that the polarization ratio undergoes a polarity transition when the field is increased. When the field continues to grow after the polarization ratio reaches its peak value, the polarization ratio decreases to zero, and then increases in absolute value but with a reversed sign.

We have also calculated several other exciton states associated with the CB1 electron states at some electric field strength. The 11H 1s state exciton has the largest oscillator strength and very small polarization ratio at a moderate field. For example, the oscillator strength for $[1\bar{1}0]$ ($[110]$) polarization is $24.64\ (24.63)\times10^{-5}$ Å^{-2}, and the ratio is as low as 2.2×10^{-4} at the field 3.65×10^4 V/cm for the sample mentioned above. On the other hand, both the 11L 2p and 12H 1s excitons, forbidden without the field, are getting oscillator strength in the range of $(0.4-1.2)\times10^{-5}$ Å^{-2} at the same field as above and they have large polarization ratios with $P_{x'y'}=0.114$, and 0.086, respectively. Like the 21L 2p state, both have strong hole mixing and their dominant and optically active components do not coincide. However, these two excitons are forbidden without the field. Actually, the differences between the oscillator strengths along two polarization directions in all three cases are of the same order of magnitude, i.e., $(0.2-0.4)\times10^{-5}$ Å^{-2}, but the polarization ratios for the forbidden ones are much larger.

In our calculations for polarization ratios, two approximations are tried and their validity examined. One is to neglect the spin splitting of the superlattice conduction subbands, namely, to combine two spin-split electron states as a one-component function; thus the exciton has only four components. The obtained exciton binding energies, oscillator strengths, and polarization ratios are very close to the corresponding results obtained when the conduction subband nondegeneracy has been fully included. The second approximation is neglecting the q dependence of the wave functions. We have also calculated $P_{x'y'}$ including the q dependence for one exciton state and found little difference in the polarization ratio, although the binding energy is reduced significantly and oscillator strength decreased somewhat. Both approximations are found to be valid.

VI. DISCUSSIONS AND CONCLUSION

In comparison with the experiments reported in Ref. 1, our numerical results also show a very small polarization ratio for the allowed 11H ground state exciton and a very similar variation trend of the polarization ratio of the 21H ground state with the electric field strength. We found that the maximum value of $P_{x'y'}$ can be as high as 60%. However, there is a serious disagreement. Our theoretical value for the critical field strength at which the polarization ratio of the 21H 1s-state exciton reaches a maximum value is much smaller than the experimental one. The theory predicts it at about 1×10^3 V/cm, while the experimental estimate is at about 2×10^4 V/cm. Although inhomogeneous broadening due to the interface roughness of the sample and the uncertainty of the applied field may widen out our narrowly peaked spectrum in Fig. 8(a), it is still quite different from the experiment.

As pointed out in Ref. 1, there are two basic contributions to $I_{\|}^{-}$ (i.e., the difference of the oscillator strengths between [110] and $[1\bar{1}0]$ polarizations). One is the coupling between the $\Gamma_{7,8}^{c}$ and the Γ_{1}^{c} band, which actually corresponds to our Rashba term B'. In the latter part of the paper the authors did not believe it of importance. Another basic contribution comes from the fact that the lattice contribution to the electro-optic effect

couples HH1 and LH1, which corresponds to our $d\epsilon$ term in Eq. (30).

In fact, our calculations have included two such terms. To examine the role played by the above terms separately, we compare the exciton polarization ratio with and without the Rashba terms. Among the two Rashba terms, B' is much smaller than R. eFB' is estimated to be -13 meV Å for a field of 3.65×10^4 V/cm. For the wave numbers which make main contribution to the exciton, $eFB'k$ is estimated to be less than 1 meV. Though B' breaks the remaining symmetry of the pair of states of θ and $\pi/2-\theta$, it could not contribute a lot to the giant Pockels effect. It can be seen that there is little difference between the binding energies, the oscillator strengths, and the polarization ratio of the 21H $1s$ exciton with and without the electric-field-induced band coupling. For instance, the binding energy of the 21H $1s$ state in both cases (excluding the q dependence of the wave functions, the same electric field and sample as in the last two paragraphs) is 8.50 meV; the calculated oscillator strengths (including the Rashba term) are 1.449×10^{-5} Å^{-2} ($[1\bar{1}0]$ polarization) and 1.402×10^{-5} Å^{-2} ([110] polarization), and the corresponding data (excluding the Rashba term) are 1.452×10^{-5} Å^{-2} ($[1\bar{1}0]$ polarization) and 1.404×10^{-5} Å^{-2} ([110] polarization); the polarization ratio is nearly the same. We have also checked the importance of the $d\epsilon$ in enhancing the Pockels effect, and found that it created about 10% relative error to ignore all the terms containing the strain ϵ. We do not think this term is responsible for so large an enhancement either.

What were not included in our calculations are the X band, the wave vector dependence of the optical matrix element $\overline{P}$ (equivalently, the number of basis functions in the $\mathbf{k} \cdot \mathbf{p}$ Hamiltonian, eight in the paper, is not enough), and the possible asymmetry occurring in the experimental samples. However, most interesting, as communicated by Kwok, till now the giant electrodichroism has only been observed in the PL spectrum, not in the PL excitation or absorption spectrum.[32] There might be some extrinsic contributions. As we all know, a PL process includes excitation, relaxation, and recombination, and is more complex than a simple process. Many kinds of scattering centers will contribute to the distribution of the recombination pair. If such a large Pockels effect is indeed an intrinsic process it will more easily be observed in the PL excitation as well as absorption spectra rather than in the weak PL from an excited state.

In conclusion, based on a bulk 8×8 multiband Hamiltonian in which the inversion-asymmetry effects are fully taken into account, we present an effective Hamiltonian for electron and hole up to the third order, in which various inversion-asymmetry factors are included. Thus we have developed a calculation method and presented results on the effects of the inversion asymmetry on the MQW hole and electron subband structures. The symmetry properties in such structures are presented. The amount as well as the in-plane anisotropy of the spin splitting of an originally twofold degenerate state are evaluated, with the emphasis put on the influence of the hole mixing. Then the polarization dependence of the hole-electron optical transition in a $GaAs/Ga_{1-x}Al_xAs$ MQW are presented, demonstrating how the hole mixing leads to a significant enhancement of the Pockels effect compared with the bulk materials. Then according to the spin-split states, we construct the theory for the exciton state an eight-component spinor. The inversion-asymmetry effects on the exciton states, especially on the optically active components, are discussed. Our numerical results for the electric field dependence of the polarization ratio for several exciton states in quantum wells clearly indicate that exciton states such as 21L $2p$, 11L $2p$, and 12H $1s$, which have strong hybridization of the heavy and light holes and have different dominant and optically active components, have the most remarkable polarization spectra when they are dipole forbidden without the electric field. The spectrum of the 21H $1s$ exciton state with the electric field is also calculated and qualitatively agrees with the experiment, but the critical field at which the polarization ratio is peaked is an order of magnitude smaller than the experimental value. Possible reasons for such disagreement are discussed.

ACKNOWLEDGMENTS

The authors are grateful to S. H. Kwok for helpful discussion. One of the authors (B.F.Z.) would like to thank Professor Lu J. Sham for his hospitality during B.F.Z.'s visit at UCSD where part of the paper was completed. This work was supported by ONR N00014-89-J-1157 and N00014-90-J-1267.

*Permanent address: Institute of Semiconductors, Chinese Academy of Sciences. P.O. Box 912, Beijing 100083, China.

[1] S. H. Kwok, H. T. Grahn, K. Ploog, and R. Merlin, Phys. Rev. Lett. **69**, 973 (1992).

[2] J. F. Nye, *Physical Properties of Crystals* (Clarendon, Oxford, 1985), Chap. 13.

[3] G. L. Bir and G. E. Pikus, *Symmetry and Strain-Induced Effects in Semiconductors* (Wiley, New York, 1974).

[4] E.g., M. Cardona, N. E. Christensen, and G. Fasol, Phys. Rev. B **38**, 1806 (1988).

[5] E. O. Kane, in *Semiconductors and Semimetals,* edited by R. K. Willardson and A. C. Beer (Academic, New York, 1966), Vol. 1, p. 75.

[6] J. M. Luttinger, Phys. Rev. **102**, 1030 (1956).

[7] M. Altarelli, J. Lumin. **30**, 472 (1985).

[8] G. Bastard and J. A. Brum, IEEE J. Quantum Electron. **QE-22**, 1625 (1986).

[9] L. J. Sham, Surf. Sci. **174**, 105 (1986); Superlatt. Microstruct. **5**, 335 (1989); L. J. Sham and Y. T. Lu, J. Lumin. **44**, 207 (1989).

[10] H. Tang and K. Huang, Chin. J. Semicond. **8**, 1 (1987) [Chin. Phys. **8**, 1101 (1987)].

[11] P. O. Lowdin, J. Chem. Phys. **19**, 1396 (1951).

[12] U. Rossler, Solid State Commun. **49**, 943 (1984).

[13] H. R. Trebin, U. Rossler, and R. Ranvand, Phys. Rev. B **20**, 686 (1979).

[14]M. H. Weiler, R. L. Aggarwal, and B. Lax, Phys. Rev. B **17**, 3269 (1978).
[15]Yu. A. Bychkov and E. I. Rashba, J. Phys. C **17**, 6039 (1984).
[16]G. Lommer, F. Malcher, and U. Rossler, Phys. Rev. B **32**, 6965 (1985); F. Malcher, G. Lommer, and U. Rossler, Superlatt. Microstruct. **2**, 267 (1986).
[17]D. Richards, B. Juserand, H. Peric, and B. Etienne, Phys. Rev. B **47**, 16 028 (1993).
[18]R. Lassnig, Phys. Rev. B **31**, 8076 (1985).
[19]R. Ferreira and G. Bastard, Phys. Rev. B **43**, 9687 (1991).
[20]J. B. Xia and K. Huang, Acta Phys. Sin. **37**, 1 (1988) [Chin. Phys. **9**, 303 (1989)].
[21]B. F. Zhu, Phys. Rev. B **38**, 13 316 (1988).
[22]J. M. Luttinger and W. Kohn, Phys. Rev. **97**, 869 (1955).
[23]*Semiconductors. Physics of Group IV Elements and III-V Compounds*, edited by O. Madelung, M. Schulz, and H. Weiss, Landolt-Börnstein, New Series, Group III, Vol. 17, Pt. a (Springer, Berlin, 1982).
[24]A. Blacha, H. Presting, and M. Cardona, Phys. Status Solidi B **126**, 11 (1984). Though given in this reference are the theoretical values of $d'^{v,cs}$ and $d'^{v,cp}$, i.e., values without the internal displacement ξ, it is easy to get $d^{v,cs}$ ($d^{v,cp}$) by subtracting $\xi d_0^{v,cs}$ (or $\xi d_0^{v,cp}$; both are corresponding optical phonon deformation potential constants).
[25]J. Callaway, *Quantum Theory of the Solid State* (Academic, New York, 1976).
[26]Of course, spin splitting is fulfilled via the spin-orbit interaction. For a superlattice electron in the presence of the electric field, if we do not take the T' and U' terms into account, such a double degeneracy remains.
[27]In calculation of these 12 valence subband dispersion and wave functions, 16 valence zero-order subband basis functions are used.
[28]B. F. Zhu (unpublished). It should be pointed out that there was a misprint in the combination coefficients for two spin-split hole states in Ref. 21. The correct ones should be $c_1\psi_\nu + c_2\psi_{\bar{\mu}}$ and $c_1\psi_\nu - c_2\psi_{\bar{\mu}}$ rather than $c_2\psi_\nu - c_1\psi_{\bar{\mu}}$.
[29]B. F. Zhu and K. Huang, Phys. Rev. B **36**, 8102 (1987); B. F. Zhu, *ibid.* **37**, 4689 (1988).
[30]H. Y. Chu and Y. C. Chang, Phys. Rev. B **39**, 10 861 (1989).
[31]L. C. Andreani and A. Pasquarello, Europhys. Lett. **6**, 259 (1988).
[32]S. H. Kwok (private communication).